Front. Energy Power Eng. China 2008, 2(3): 243–248
DOI 10.1007/s11708-008-0049-7

RESEARCH ARTICLE

Fenghao WANG, Gedong JIANG, John Zhang Lin

Simulation of cross-flow-induced vibration of tube bundle by surface vorticity method

Abstract A fluid-structure interaction model based on Surface Vorticity Method (SVM) was used to study flow-induced vibrations of tube bundles in medium space ratio. The flow-induced vibrations of four tubes in a rotated square and a staggered tube bundle in three-row and five-column arrangements were simulated in the high sub-critical Reynolds number (*Re*) range. The results on fluid forces, tube responses and vorticity maps were presented. The vorticity maps of the four rotated-square tubes changed dramatically when the rigid tubes were replaced by the flexible tubes. From the vorticity maps and vibration responses of the staggered tube bundle of different structural parameters, it was found that with the decrease of tube natural frequency, the maximal vibration response moved from the third row to the first. The results also showed that when more flexible tubes are used, the flow pattern changed drastically and the fluid-structure interaction imposed a dominant impact on the flow.

Keywords flow-induced vibration, fluid-structure interaction, tube bundle, surface vorticity method

1 Introduction

Tube bundle failures due to cross-flow-induced vibrations are a catastrophic event in the heat exchanger of a nuclear steam generator. Characterized by high Reynolds numbers and unsteady flow, the flow-induced vibrations (FIV) of the tube bundles are very complex. Over the past years, many investigations have been made and many papers have been published to explain this phenomenon [1–7].

Apart from the extensive efforts made on this problem based on experiments and computational fluid dynamics (CFD), research on FIV of tube bundles has thrived only in the past ten years with the rapid development of computer technology and computational methods. For mesh-based CFD methods, almost all simulations related to FIV are limited to low Reynolds numbers € and small numbers of cylinders [8–11]. Considering the computational difficulty and cost due to mesh remapping, it is prohibitive to use mesh-base CFD method in engineering practice.

A mesh-free method such as the vortex method is a natural and computationally less expensive approach for the simulation of turbulent flows. This method is especially suitable for flow-induced vibration problems because structures in the simulation can move freely over a large distance. Lam et al [12] proposed a fast and practical mesh-free computational method based on surface vorticity method (SVM) for FIV of multi-cylinders at sub-critical *Re* range. With this method they simulated the FIV of a single flexible cylinder and two flexible cylinders at high sub-critical *Re*. The objective of the present investigation is to use this fast method to examine the fluid-structure interaction of the tube bundles in cross flow.

For the calculation, natural frequency of the tube is described by f_n, the reduced damping parameter which represents flexibility. Damping of the tubes is defined as $S_G = 8\ \pi^2 St^{*2} M\xi$, where $St^* = f_0 D/U$ is the Strouhal frequency (it is about 0.21 at high sub-critical *Re* range) which is determined by f_0 (the shedding frequency of a single rigid cylinder), the mainstream velocity U and the tube diameter D. $M = m/(\rho D^2)$ is the mass ratio, which is determined by m (the tube mass per unit length), the fluid density ρ and D. $\zeta = c/\left(2\sqrt{km}\right)$ is the tube damping ratio defined by the damping coefficient c and the equivalent stiffness k and m.

Received December 14, 2007; accepted January 28, 2008

Fenghao WANG (✉)
School of Human Settlements and Civil Engineering, Xi'an Jiaotong University, Xi'an 710049, China
E-mail: fhwang@mail.xjtu.edu.cn

Gedong JIANG
School of Mechanical Engineering, Xi'an Jiaotong University, Xi'an 710049, China

John Zhang Lin
Division of Building Science and Technology, City University of Hong Kong, Hong Kong, China

2 FIV of configuration of four tubes arranged in rotated square

The four square tube bundle arrangement is a basic unit that can often be seen in heat exchangers. Previous experiments [13–16] revealed that the flow pattern of the four tubes in square configuration is far more complex than that of a single cylinder, since the shedding frequency and the mean/fluctuation force are strongly influenced by the main stream direction and the space ratio. For flexible tubes, the coupling of the fluid and the vibration response of the four tubes further complicates the flow pattern.

Figure 1 is the layout of the four tubes in rotated square configuration. The simulations are conducted at $L/D = 2.0$, where L is the edge length of the square and $Re = 2.67 \times 10^4$ for rigid and flexible tubes. The parameters of the flexible tubes are chosen as $f_n/f_0 = 1.0$, $S_G = 1.29$ and 0.615 (corresponding to $M = 10$ and 4).

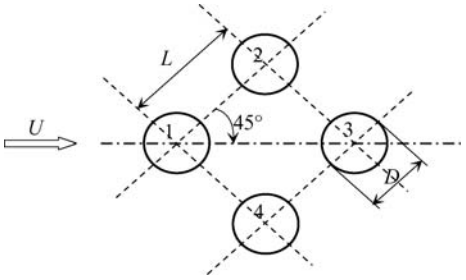

Fig. 1 Schematic layout of four tubes in rotated square configuration

2.1 Flow pattern and fluid force

The calculated and experimental results [13,16] on flow force coefficients and Strouhal frequency $St = f_s D/U$ (defined by shedding frequency f_s) of the four rigid tubes in rotated square configuration are shown in Table 1. The computational mean and fluctuation force coefficients reflect some basic flow features of the four rotated square arranged tubes in medium space ratio ($L/D = 2.0$) in agreement with experimental results. Influenced by the gap action of the two side tubes (tubes 2 and 4), the wake of tube 1 is narrow and tube 3 is directly impinged by the vortices shedding from tube 1 (Fig. 2(a)). Hence the mean drag coefficient ($\bar{C}_D$) of tube 1 is slightly smaller than that of a single cylinder (The drag coefficient of a single cylinder is about 1.2 in the sub-critical Reynolds number range). The mean drag coefficient of tube 3 is half of that of a single cylinder and the mean drag coefficients of tubes 2 and 4 are close to that of a single cylinder. The signs of the mean lift coefficients ($\bar{C}_L$) of tubes 2 and 4 are opposite and their absolute values are larger than those of tubes 1 and 3. Both the lift and drag fluctuation coefficients (C'_D, C'_L) of tube 1 are the smallest among the four tubes, while the lift fluctuation coefficient of tube 3 is the largest among the four tubes. Similar to experimental results [16], the Strouhal frequency is about 0.27 in the calculation. The other Strouhal frequency in the simulation is 0.18, which is about half that in the experimental results (0.38–0.40) [16]. This discrepancy could be caused by the following two reasons. First, the simulation is performed in an unbounded flow field while the experiment is conducted in the water tunnel where the block effect is unavoidable. Second, the calculation is two-dimensional while in the experiment the flow is three-dimensional.

As the tubes are moving, the flow pattern of the four rotated square tubes in medium space ratio varies at different reduced damping parameters. The flow pattern of the flexible tubes at $S_G = 1.29$ is almost the same as that of the rigid tubes (Fig. 2(b)), while the flow pattern of the flexible tubes at $S_G = 0.516$ changes dramatically as the tubes depart significantly from the initial position (Fig. 2 (c)). The departures of the tubes interrupt the gap action of tubes 2 and 4, which result in no direct vortices shedding from tube 1 to impinge on tube 3. The flow modes are also reflected in the force coefficients and Strouhal frequency (shown in Table 2). ① At $S_G = 1.29$, the absolute values of the force coefficients increase compared with rigid tubes, provided that the relative relations of the force in the four tubes remain the same, except that the mean lift coefficients of tubes 1 and 3 are larger than those of tubes 2 and 4. ② At $S_G = 0.516$, the mean drag coefficients of tubes 1, 2 and 4 decrease compared with their rigid counterparts, and the fluctuation force

Table 1 Force coefficients and Strouhal frequency of four rigid tubes in rotated square configuration

	present results				experimental results							
	$L/D = 2.0$, $Re = 2.67 \times 10^4$				Lam & Fang (1995)				Lam et al (2003)			
					$L/D = 2.02$, $Re = 1.28 \times 10^4$				$L/D = 2.11$, $Re = 4.1 \times 10^4$			
	$\bar{C}_D$	C'_D	$\bar{C}_L$	C'_L	$\bar{C}_D$	C'_D	$\bar{C}_L$	C'_L	$\bar{C}_D$	C'_D	$\bar{C}_L$	C'_L
tube 1	0.88	0.04	0.08	0.17	0.92	–	−0.02	–	1.01	0.06	0.00	0.15
tube 2	1.19	0.11	−0.13	0.28	1.18	–	−0.11	–	1.32	0.17	−0.21	0.20
tube 3	0.48	0.49	−0.06	0.65	0.57	–	−0.01	–	0.45	0.15	−0.08	0.60
tube 4	1.28	0.15	0.23	0.33	1.18	–	0.09	–	–	–	–	–
St^*	0.24–0.27 0.18				–				0.26–0.27 0.38–0.40			

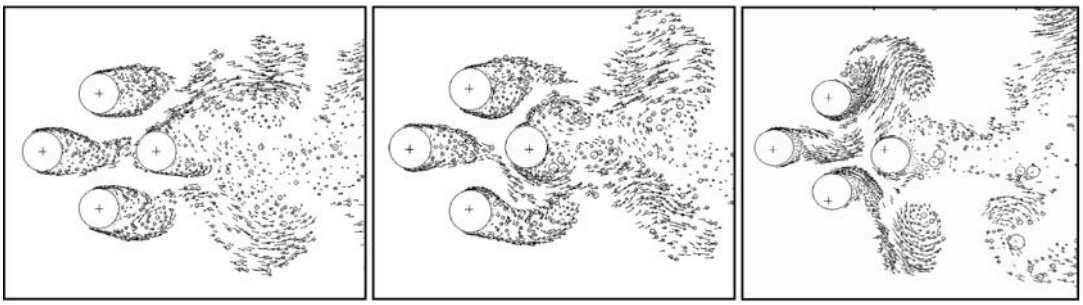

Fig. 2 Vorticity map of four tubes in rotated square configuration
(a) Rigid; (b) $S_G = 1.29$ and $M = 10$; (c) $S_G = 0.516$ and $M = 4$(The cross is the initial centre of the tube, and the initial configuration of the four tubes is rotated square of $L/D = 2.0$)

Table 2 Force coefficients and Strouhal frequency of four tubes in rotated square configuration $L/D = 2.0$ at different reduced damping parameters

	rigid				$S_G = 1.29$				$S_G = 0.516$			
	$\bar{C}_D$	C'_D	$\bar{C}_L$	C'_L	$\bar{C}_D$	C'_D	$\bar{C}_L$	C'_L	$\bar{C}_D$	C'_D	$\bar{C}_L$	C'_L
tube 1	0.88	0.04	0.08	0.17	1.10	0.13	−0.10	0.22	1.04	0.28	0.00	0.32
tube 2	1.19	0.11	−0.13	0.28	1.46	0.18	−0.07	0.32	1.12	0.64	0.20	1.07
tube 3	0.48	0.49	−0.06	0.65	0.66	0.55	0.15	0.74	0.55	0.64	0.04	1.04
tube 4	1.28	0.15	0.23	0.33	1.55	0.19	0.06	0.42	1.16	0.56	−0.01	0.76
St^*	0.18 0.24–0.27				0.17–0.19 0.26–0.28				0.16–0.18			

coefficients of tubes 2 and 4 are close to that of tube 3. ③ At $S_G = 1.29$, the Strouhal frequency at around 0.27 and 0.18 are both seen in the vibrating tubes, while at $S_G = 0.516$, only the Strouhal frequency at around 0.18 occurs.

2.2 Vibration response and tube locus

With the variations of the reduced damping parameter, the vibration responses of the four tubes in rotated square configuration are also changed. Figures 3 and 4 are the loci of the four tubes at $S_G = 1.29$ and $S_G = 0.615$ respectively. At $S_G = 1.29$, the vibrations in y direction are larger than those in x direction for all the tubes except tube 3, and the maximum vibration amplitude (r.m.s. $0.046D$) is in x direction of tube 3. At $S_G = 0.615$, the vibration amplitude in y direction is larger than that in x direction for all the tubes except tube 1, and the maximum amplitude (r.m.s. $0.163D$) is in y-direction of tube 2. Compared with the vibration amplitudes of the four tubes at $S_G = 1.29$, the vibration amplitudes and the departures from their initial positions of the four tubes at $S_G = 0.615$ are all increased, which means that the interactions between fluid and tubes

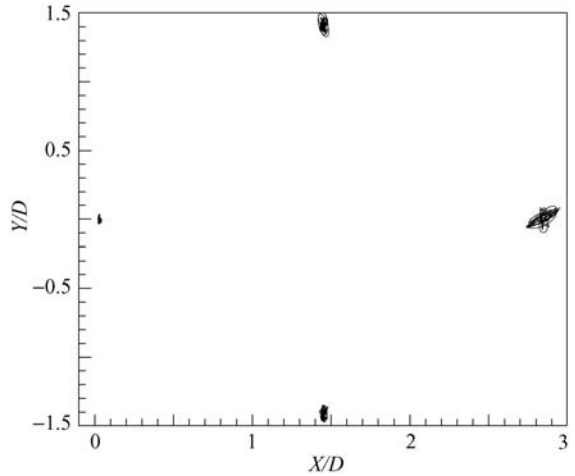

Fig. 3 Locus of four vibrating tubes in rotated square configuration at $S_G = 1.29$ and $M = 10$

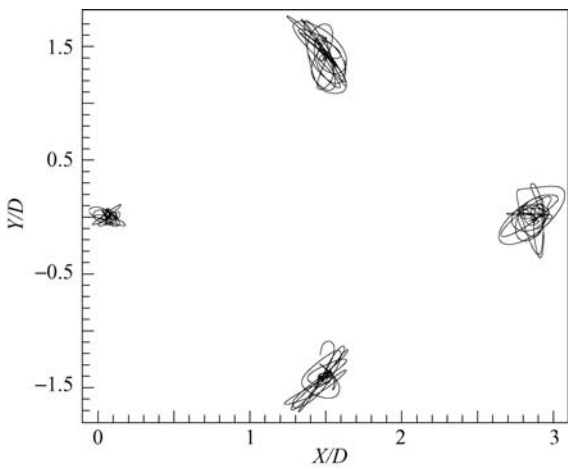

Fig. 4 Locus of four vibrating tubes in rotated square configuration at $S_G = 0.516$ and $M = 4$

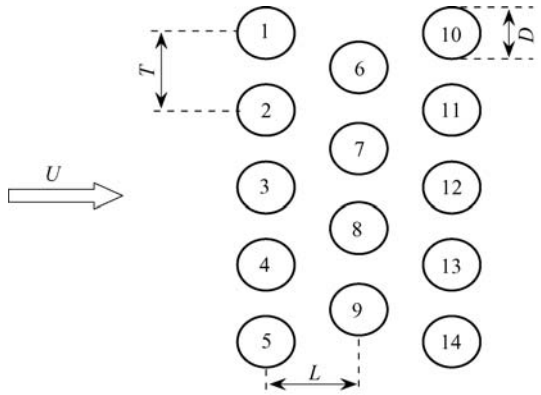

Fig. 5 Schematic layout of staggered tube bundle, $T/D = L/D = 2.0$

are strengthened for the four tubes in rotated square configuration when reduced damping parameter decreases from $S_G = 1.29$ to $S_G = 0.615$.

3 Cross-flow-induced vibration of staggered tube bundle

The cross-flow past a staggered tube bundle of three rows ($T/D = L/D = 2.0$, where L is the distance between two rows and T is the distance between two tubes in one row, with four or five tubes in each row as shown in Fig. 5) is simulated tentatively only in y direction at $Re = 2.67 \times 10^4$ for rigid tubes and for flexible tubes of $S_G = 1.29$ and, $f_n/f_0 = 1.0$ and 2.0.

Figure 6 is the comparison of the vorticity maps under different conditions. It can be seen that when the tubes are all rigid, the flow around the tubes is regular (Fig. 6(a)). The wakes produced by the tubes in the first row are narrowed by the gap between the tubes in the second row, while the wakes produced by the tubes in the second row are wider. In the third row, there are wide and narrow wakes: the wide wakes are formed behind tubes 11, 13 and 15, while the narrow wakes are formed behind tubes 10 and 12. The force frequency analysis of the tubes in different rows is consistent with the vorticity distribution, i.e., the narrow wake of the first row corresponds to a shedding frequency of 0.26, the wide wake of the second row to 0.17, and the third row to 0.26 and 0.12. These data show that the shedding frequency in the first row is larger than that of the second row, which conforms to the experimental results of Oengoren & Ziada [17] at flow past a normal triangular tube array of $P/D = 2.08$ (where P is the edge length of the normal triangular) at $Re = 1800$.

The vorticity map of the flexible tube bundle at $f_n/f_0 = 2{\cdot}0$ (Fig. 6(b)) is slightly different from that of the rigid tubes, but the whole flow pattern is similar. The flow-induced vibrations in this case are quite small (Fig. 7), the vibration responses are increased along the stream direction, and the maximal vibration amplitude $0.06D$ occurs at tube 11 in the third row.

The vorticity map of the flexible tube bundle at $f_n/f_0 = 1{\cdot}0$ (Fig. 6(c)) is quite different from that of rigid tubes. Due to the large-amplitude vibrations in the first row (Fig. 8), jet flow occurs between tubes 3 and 4, which makes the flow past the tube bundle violently. In contrast to the situation of $f_n/f_0 = 2.0$, the vibration responses of the tubes decrease along the stream direction, and the maximal vibration amplitude $0.69D$ occurs at tube 3 in the first row.

Compared with the vibration responses in the two flexible tube bundle cases ($f_n/f_0 = 1.0$ and 2.0 respectively), fluid-structure interaction is unnoticeable for small-amplitude vibrations, hence the influence of the tubes vibrations to the fluid field can be neglected. But for large-amplitude vibrations, the fluid-structure interaction is obvious, which implies that the influence of the tube vibrations to the fluid field is significant.

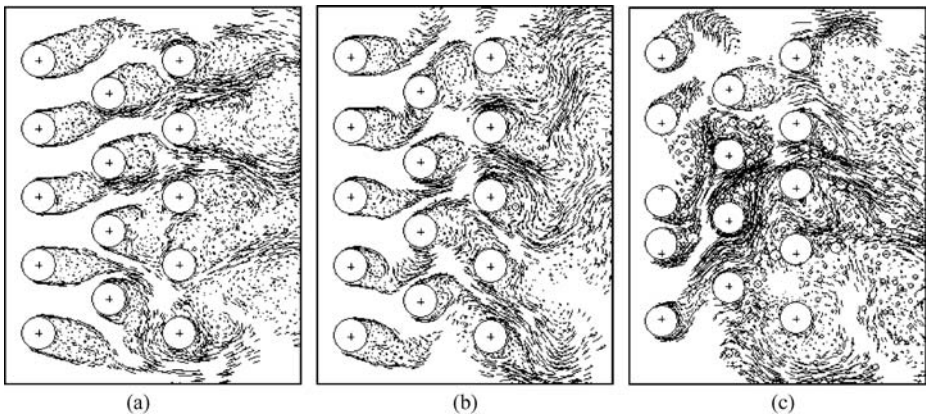

Fig. 6 Vorticity map of flow past staggered tube bundle
(a) Rigid tubes; (b) flexible tubes at $S_G = 1.29$ and $f_n/f_0 = 2.0$; (c) flexible tubes at $S_G = 1.29$ and $f_n/f_0 = 1.0$

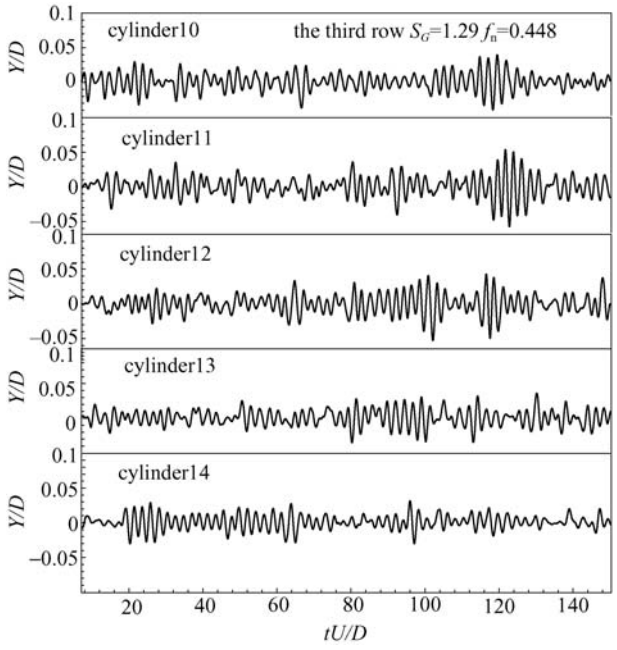

Fig. 7 Flow-induced vibration in third row of staggered tube bundle at $f_n/f_0 = 2.0$

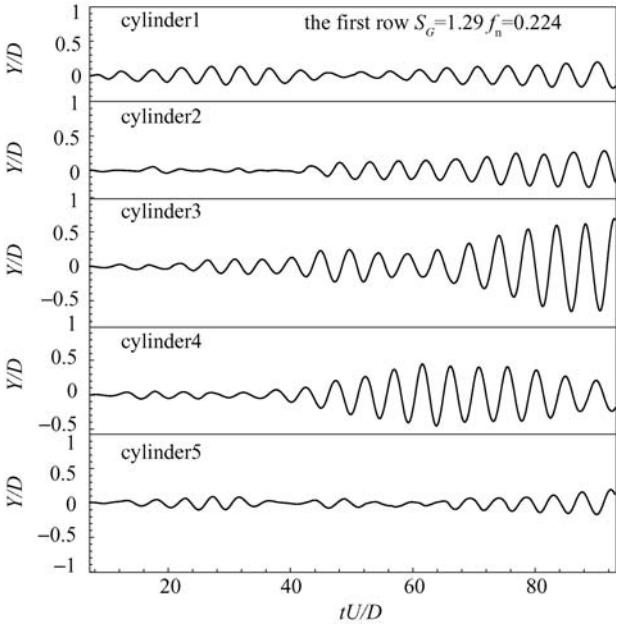

Fig. 8 Flow-induced vibration in first row of staggered tube bundle at $f_n/f_0 = 1.0$

4 Conclusion and discussion

A fluid-structure interaction model based on SVM is used to study FIV of tube bundles in medium space ratio at $Re = 2.67 \times 10^4$. The FIV of four tubes in rotated square arrangement are simulated. This model is then applied to simulate a staggered tube bundle of three rows at similar Reynolds numbers. It is shown that with the large departure from the initial position at the small reduced damping parameter, the vorticity maps of the four tubes change dramatically. With the decrease of tube natural frequency, the maximal vibration response of the staggered tube bundle changes from the third row to the first. For the more flexible tube case, the vorticity map of the tubes changes violently and the fluid-structure interactions are significant. The simulation results of FIV of tube bundle at sub-critical Reynolds numbers using the current method are promising and reasonable.

It is well known that in a small space ratio, the fluidelastic instability caused by FIV is predominant in a tube bundle. For medium to large space ratios, large-amplitude vibrations of the tube bundle caused by vortex shedding become the main reason for the tube bundle failure. As a result, the fluidelastic characteristics are no longer important for the tube bundle. Hence, only flow-induced vibrations in medium space ratio are covered in this paper. There are still some discrepancies between current simulation and the experimental results. In the current calculation, the flow field around the tube bundle is supposed to be an unbounded duct, which is certainly different from the boundary condition outlined by a bounded duct in the experiment. For the medium space ratio, this assumption is acceptable, but for the small space ratio, this assumption could have been wrong. To simulate the fluidelastic instability of tube bundles in a small space ratio by SVM, the most difficult task lies in how to add wall panels to the flow field. The authors of this paper tried the image method and periodical method, but both methods failed. Once this difficulty is overcome, it would be hopeful that with this relatively simple and computationally inexpensive method, fluidelastic instability of tube bundles of different configurations in heat exchange can be simulated at high sub-critical Reynolds numbers.

Acknowledgements The authors gratefully acknowledge the financial support from the National Natural Science Foundation of China (Grant No. 50506022).

References

1. Paidoussis M P. A review of flow-induced vibrations in reactor and reactor components. Nuclear Engineering Design, 1983, 74: 31–60
2. Weaver D S, Fiztpatrick J A. A review of cross-flow induced vibrations in heat exchanger tube arrays. Journal of Fluids & Structure, 1988, 2: 73–93
3. Moretii P M. Flow-induced vibrations in arrays of cylinders. Annual Review of Fluid Mechanics, 1993, 25: 99–114
4. Blevins R D. Flow-Induced Vibrations. 2nd Edition. Florida: Krieger, 1994
5. Price S J. A review of theoretical models for fluid-elastic instability of tubes in cross-flow. Journal of Fluids & Structure, 1995, 9: 463–518

6. Chen S S, Srikantiah G S. Motion-dependent fluid force coefficients for tube arrays in Crossflow. ASME Journal of Pressure Vessel Technology, 2002, 123(4): 429–436
7. Tanaka T, Tanaka K, Shimizu F. Fluidelastic analysis of tube bundle vibration in cross-flow. Journal of Fluids & Structure, 2002, 16(1): 93–112
8. Ichioka T, Kawata Y, Nakamura T, et al. Research on fluid elastic vibration of cylinder arrays by computational fluid dynamics (Analysis of two cylinders and a cylinder row). JSME International Journal, Series B: Fluid and Thermal Engineering, 1997, 40(1): 16–24
9. Kassera V, Strohmeier K. Simulation of tube bundle vibrations induced by cross-flow. Journal of Fluids & Structure, 1997, 11: 909–928
10. Schroder K, Gelbe H. Two- and three-dimensional CFD-simulation of flow-induced vibration excitation in tube bundles. Chemical Engineering Processing, 1999, 38: 621–629
11. Liu Y, So R M C, Lau Y L, Zhou Y. Numerical studies of two side-by-side elastic cylinders in a cross-flow. Journal of Fluids & Structure, 2001, 15: 1009–1030
12. Lam K, Jiang G D, Liu Y, et al. Grid-free surface vorticity method applied to flow induced vibration of flexible cylinders. International Journal for Numerical Method in Fluids, 2004, 46: 289–313
13. Lam K, Lo S C. A visualization study of cross-flow around four cylinders in a square configuration. Journal of Fluids & Structure, 1992, 6: 109–131
14. Lam K, Fang X. The effect of interference of four equispaced cylinders in cross flow on pressure and force coefficient. Journal of Fluids & Structure, 1995, 9: 195–214
15. Lam K, Li J Y, Chan K T, et al. Flow pattern and velocity field distribution of cross-flow around four cylinders in a square configuration at low Reynolds number. Journal of Fluids & Structure, 2003, 17(5): 665–675
16. Lam K, Li J Y, So R. M. C. Force coefficients and Strouhal numbers of four Cylinders in cross-flow. Journal of Fluids & Structure, 2003, 18(3–4): 305–324
17. Oengoren A, Ziada S. An in-depth study of vortex shedding acoustic resonance and turbulent forces in normal triangular tube arrays. Journal of Fluids & Structure, 1998, 12: 717–758